DOI: 10.1002/ ((please add manuscript number))

Article type: Research Article

Title: Performance of PEDOTOH/PEO-based supercapacitors in agarose gel electrolyte

Author(s), and Corresponding Author(s)*

Shofarul Wustoni[a,b,*], Georgios Nikiforidis[c], David Ohayon[d], Sahika Inal[d], Yuli Setyo Indartono[b], Veinardi Suendo[a], and Brian Yuliarto[b,*]

[a]*Department of Chemistry, Institut Teknologi Bandung (ITB), Bandung 40132, Indonesia.*

[b]*Research Center for New and Renewable Energy, ITB, Bandung 40132, Indonesia.*

[d]*UCL Institute for Materials Discovery, University College London, Malet Place, London WC1E 7JE, United Kingdom.*

[d]*Biological and Environmental Science and Engineering Division, King Abdullah University of Science and Technology (KAUST), Thuwal 23955-6900, Saudi Arabia.*

Keywords: PEDOT, Electropolymerization, Agarose, Gel Electrolyte, Supercapacitors.

Abstract:

Poly(3,4-ethylenedioxythiophene) (PEDOT) is a prime example of conducting polymers materials for supercapacitors electrodes that offer ease of processability and sophisticated chemical stability during operation and storage in aqueous environments. Yet, continuous improvement on its electrochemical capacitance and stability upon long cycles remains a major interest in the field, such as the developing PEDOT-based composites. This work evaluates the electrochemical performances of hydroxymethyl PEDOT (PEDOTOH) coupled with hydrogel additives, namely poly(ethylene oxide) (PEO), poly(acrylic acid) (PAA), and polyethyleneimine (PEI), fabricated *via* a single-step electrochemical polymerization method in an aqueous solution. The PEDOTOH/PEO composite exhibits the highest capacitance (195.2 F g^{-1}) compared to pristine PEDOTOH (153.9 F g^{-1}), PEDOTOH/PAA (129.9 F g^{-1}), and PEDOTOH/PEI (142.3 F g^{-1}) at a scan rate of 10 mV s^{-1}. The PEDOTOH/PEO electrodes were then assembled into a symmetrical supercapacitor in an agarose gel. The type of supporting electrolytes and salt concentrations were further examined to identify the optimal agarose-based gel electrolyte. The supercapacitors comprising 2 M agarose-$LiClO_4$ achieved a specific capacitance of 27.6 F g^{-1} at a current density of 2 A g^{-1}, a capacitance retention of ~94% after 10,000 charge/discharge cycles at 10.6 A g^{-1}, delivering a maximum energy and power densities of 11.2 Wh kg^{-1} and 3.45 kW kg^{-1}, respectively. The performance of the proposed supercapacitor outperformed several reported PEDOT-based supercapacitors, including PEDOT/carbon fiber, PEDOT/CNT, and PEDOT/graphene composites. This study provides insights into the effect of incorporated hydrogel in the PEDOTOH network and the optimal conditions of agarose-based gel electrolytes for high-performance PEDOT-based supercapacitor devices.

Keywords: PEDOT, Hydrogels, Electropolymerization, Conducting Polymer, Supercapacitors, Agarose gel.

Introduction

Supercapacitors (SCs) are energy storage devices between electrolytic capacitors and rechargeable batteries. They are extensively used for various applications, such as power supply, power buffering, and energy backup systems in hybrid vehicles and consumer portable devices. Their ubiquitous use in today's electronics is due to their characteristics, namely fast charging-discharging rates (not kinetically limited as for batteries), long cycle life (>500,000 cycles), high power densities (>50 kW kg^{-1}), and broad operating temperature window (-45 to 80°C). SCs function on a physical storage mechanism (i.e., electric double-layer) and/or reversible redox reactions, which alleviates issues related to irreversible chemical reactions (that occur in batteries), and typically comprises two electrodes separated by an insulator and connected through an electrolyte.[1]

To produce high-performance SCs for practical applications, significant efforts have been directed to improve the properties of each of its components. The electrode material is the most crucial element, directly affecting the supercapacitors' performances, i.e., capacitance, long-term stability, energy, and power density. Such electrodes notably comprise (nanoporous) carbon materials, owing to their wide allotrope forms, high surface area (>2000 m^2 g^{-1}), large pore volumes (~1.2 nm), stability, intrinsic capacitance, and widely developed production at low cost.[2] Pseudocapacitors, an emerging class of SCs, utilize conducting polymer or metal oxide-based electrodes, often mixed with functionalized porous carbons, combining electrostatic and pseudocapacitive charge storage mechanisms. Amongst these electrode materials, conducting polymers, thanks to their mixed conduction and processability properties, offer excellent electrochemical performance and robust mechanical features, opening new form factors for SCs fabrication, such as flexible and stretchable energy storage devices.[3]

Poly(3,4-ethylenedioxythiophene) (PEDOT) is a prime example of conducting polymer with excellent chemical stability in various environments.[4] PEDOT electrodes in SCs have been widely demonstrated in different configurations, including fiber-based SCs, micro-supercapacitors, and flexible and stretchable SCs.[5] However, despite their robust electrochemical performance, PEDOT electrodes still possess a few drawbacks. These include a lack of structural stability under repetitive doping/dedoping processes and a relatively low specific capacitance and ion mobility compared to other pseudocapacitive materials.[5] To address these challenges, the fabrication of PEDOT-based composites has been an active field of research in recent years. A few examples include the work of Khasim et al. where the authors used graphene to synthesize secondary doped PEDOT:PSS nanocomposites.[6] Xu et al. reported PEDOT:PSS/V_2O_5 composites for hybrid fiber-based SCs.[7] Recently, the formation of PEDOT:PSS composite with 2D MXene materials has been extensively demonstrated to enhance the SCs performances.[8] On top of the above, combinations of PEDOT with inorganic materials (e.g., metal nanoparticles, 2D TMD, etc.) have been proposed to exceed the current state-of-the-art of PEDOT-based SCs.[5, 9] The obtained hierarchical structures and synergistic effect of the two components in the PEDOT composites drastically improve ion mobility and in turn, the specific capacitance by facilitating ions infiltration from the electrolyte into the electrode bulk. However, the majority of these composites entail complex synthesis steps and multiple reagents, adding to the cost and fabrication time of the process. Thus, a simpler alternative design of PEDOT-based composites is desirable to boost the electrochemical and mechanical properties of PEDOT-based SCs further.

In this direction, hydrogels are ideal candidates to pair with PEDOT composites. These gels can improve the ionic conductivity within the composites‘ bulk, enhance swelling in aqueous electrolytes, and offer mechanical robustness to incorporate the SCs into stretchable and flexible devices, as opposed to electrodes made from pristine PEDOT.[10] There are, however,

limited reports on facile synthesis methods of PEDOT composites with hydrogel for SC application. Recent examples of PEDOT/hydrogel composites for SCs include (i) PEDOT:PSS/Polyvinyl alcohol (PVA) prepared by the freeze-thaw crosslinking and solution immersion method,[10] and (ii) PEDOT:PSS/poly(acrylamide) developed through a free-radical polymerization method.[11] Yet, as mentioned earlier, these fabrication protocols involve complex and lengthy instrumental setup. Hence, it is imperative to explore straightforward methods to prepare PEDOT/hydrogel electrodes for high-performance SCs.

To this end, we explore the use of agarose as a gel electrolyte towards symmetrical SCs comprising electrodeposited PEDOT electrodes. Gel electrolytes, composed of a polymer matrix with ionic compounds (e.g., salts, acids, and bases), have been explored in recent years due to their promising physical and chemical properties such as high ionic conductivity (up to 82 mS cm^{-1})[12], smooth contact with the electrode surface, stability over long-term cycling, ease to use, as well as being environmentally friendly and safe to handle.[13] Such electrolytes correlate to the development of solid-state polymer-based electrolytes for electrochemical SCs in mobile, wearable, and computing electronics.[13] To date, different types of gel electrolytes have been demonstrated as solid-state electrolytes with excellent electrochemical performance; for instance, Senthilkumar et al., reported polyvinyl alcohol (PVA) gel electrolyte comprising H_2SO_4, assembled in a solid state electrochemical double layer capacitor (SSEDLC).[14] The supercapacitors showed a specific capacitance as high as 412 F g^{-1} and energy density of 9.16 W h kg^{-1} at 1.56 A g^{-1}. The remarkable electrochemical performance of this SC was attributed to the contribution of high ionic conductivity from the gel electrolyte and good electrode/electrolyte interface. Another example of gel electrolyte utilizing sodium salt-polyethylene oxide was performed by Ramasamy et al.[15] They reported activated carbon SC using this gel electrolyte with the cell operating at a stable potential window of 2.5 V. This SC exhibited a specific capacitance of 24 F g^{-1}, energy and power densities of 18.7 Wh kg^{-1} and

0.52 kW kg^{-1}, respectively. However, there is no report yet focusing on evaluating PEDOT/hydrogel composite electrodes with agarose gel electrolytes and the effect of ionic concentration in the gel electrolyte on the SCs performances.

Herein, we present a comparative study of electropolymerized PEDOTOH:ClO_4 composites under different hydrogels, including poly(ethylene oxide) (PEO), poly(acrylic acid) (PAA), and poly(ethylene imine) (PEI), using a single-step electrochemical polymerization. In recent years, PEO, PAA, and PEI have been extensively used as hydrogel materials in bioengineering to build smart functional materials or mixed with several organic semiconducting materials in optoelectronic devices.[16] However, literature on combining these hydrogels with PEDOT-based electrodes for SCs is limited. The successful polymerization of PEDOTOH chains and formation of the PEDOTOH/gel composites were characterized using FTIR and XPS. The electrochemical measurements reveal that the PEDOTOH/PEO (195.2 F g^{-1}) composite exhibits the highest capacitance compared to pristine PEDOTOH (153.9 F g^{-1}), PEDOTOH/PAA (129.9 F g^{-1}), and PEDOTOH/PEI (142.3 F g^{-1}) at a scan rate of 10 mV s^{-1}. Subsequently, we fabricated symmetrical SCs by combining the PEDOTOH:ClO_4/PEO electrodes with an agarose gel electrolyte upon optimizing its parameters (i.e., the type of incorporated ions and their concentration). The SC devices delivered a maximum energy density of 11.2 Wh kg^{-1} and maximum power density of 3.45 kW kg^{-1} with excellent cycling stability (~94% after 10,000 charge/discharge cycles at 10.6 A g^{-1}) in 2 M $LiClO_4$/agarose gel electrolyte. This study advances the understanding of electropolymerized PEDOT/hydrogel-based electrodes and delineated the effect of gel electrolytes for developing high-performance of PEDOT-based supercapacitors.

Results and Discussion

We designed conducting polymer composites using hydroxymethyl EDOT (EDOTOH) monomer and ClO_4^- counteranions. The EDOTOH monomer was selected as the building block of the polymer network due to better solubility in aqueous solution with higher electropolymerization efficiency than EDOT monomer, and the resulting PEDOTOH polymer films exhibited an improvement in the electrochemical properties compared to native electropolymerized PEDOT.[17] In total, three gels with different chemical functional groups were used to fabricate PEDOTOH/gel composites, including poly(ethylene oxide) (PEO), poly(acrylic acid) (PAA), and poly(ethylene imine) (PEI). The polymer composites were synthesized via a single-step electrochemical polymerization method, a robust and straightforward technique to accurately deposit polymer films on a particular electrode geometry. Accordingly, we kept all electropolymerization parameters identical and only tuned the type of hydrogel mixed in the monomer solutions. After 5-minute-long electropolymerization in deionized (DI) water, the average mass loading of 180, 237, 202, and 181 μg were deposited for PEDOTOH:ClO_4, PEDOTOH:ClO_4/PEO, PEDOTOH:ClO_4/PAA, and PEDOTOH:ClO_4/PEI films, respectively.

The formation of polymerized PEDOTOH/gel composites was characterized by FTIR and XPS measurements (**Figure 1**). As shown in **Figure 1a**, the FTIR spectra display two major peaks at 1270 and 1466 cm^{-1}, attributed to the stretching vibration mode of C=C and inter-ring stretching mode of C-C in the thiophene chain. The peak at 983 cm^{-1} corresponds to the stretching vibration of the C-S-C bond in the conjugated thiophene chain. The FTIR spectra confirmed the successful PEDOTOH polymerization, both with and without the presence of the hydrogels. Furthermore, to substantiate the incorporation of the hydrogels within the PEDOTOH network, XPS measurements were conducted (**Figure 1b**). According to the high-resolution of C 1s spectra, the PEDOTOH/PEO shows a slightly higher C-O component (19%)

than the pristine PEDOTOH (17%), indicating the contribution of C-O bonds from the PEO in the composite. Simultaneously, the presence of O-C=O and C-N are attributed to the incorporated PAA and PEI, respectively (**Figure 1b**). Notably, the high-resolution of N 1s spectra affirmed the fingerprint nitrogen elements, only observed in the PEDOTOH/PEI composite sample. Therefore, the FTIR and XPS results corroborate the PEDOTOH polymers' formation and the gel incorporation in the composites.

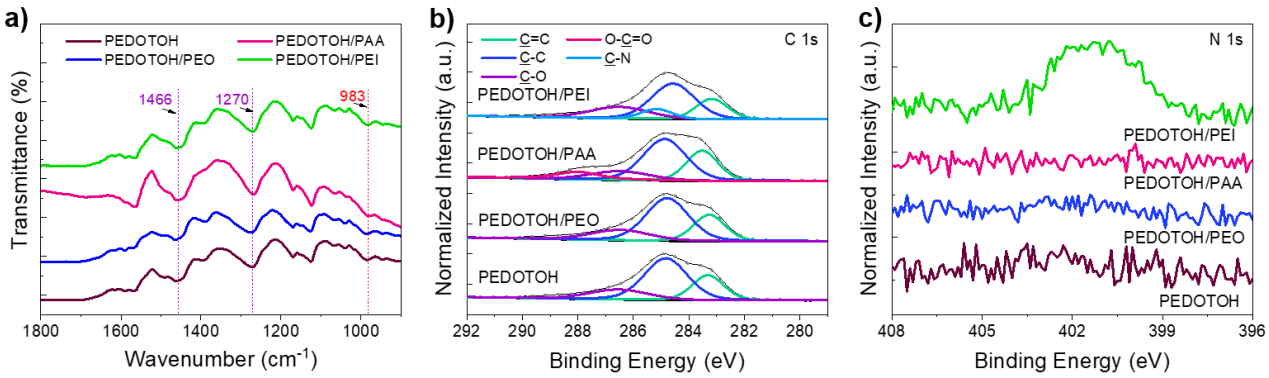

Figure 1. Physicochemical characterizations of the PEDOTOH films. **(a)** FTIR spectra of PEDOTOH films in the range of 900 cm^{-1} to 1800 cm^{-1}. The assigned peaks denote the characteristics of PEDOT polymerization. High resolution **(b)** C 1s and **(c)** N 1s XPS spectra of PEDOTOH films.

The electrochemical properties of PEDOTOH composites films coated on a flexible Au/Kapton substrate were examined with a three-electrode system in 1 M $LiClO_4$ aqueous solution by cyclic voltammetry (CV), galvanostatic charge-discharge (GCD), and electrochemical impedance spectroscopy (EIS). All the electrodes share similar CV curves at a scan rate of 10 mV s^{-1} (**Figure 2a**). The CV curves preserve a rectangular-type shape over a range of scan rates, which we analyzed further by plotting the log(current density) versus log(scan rate) (**Figure S1**). The b-value extracted from fitting the log(J) versus log(v) delineates the charge storage mechanism, where a b-value close to 1 indicates a capacitive-controlled process, while the value around 0.5 represents a diffusion-limited process. As shown in **Figure S1e-h**, the b-values of

PEDOTOH electrodes with and without the incorporated gel are 0.99, indicating an ideal capacitive-controlled process. The CV results reveal that the incorporated insulating gel does not hinder charge storage capability in the PEDOTOH networks. While the PEDOTOH incorporated PAA and PEI gels achieve similar current densities to the pristine one, the PEDOTOH/PEO generates the highest current density at the same geometrical electrode (0.64 cm^2). We postulate that the presence of PEO with significant higher number of C-O-C bonds can boost the capability of PEDOTOH networks to interact with ions and improves the water uptake from the electrolyte. This observation aligns with the established finding of the use of PEO or PEG as the primary side-chain and/or additive in the semiconducting polymer to revamp the mixed ion-electron conducting properties.[16a, b, 18] Furthermore, PEO has been widely used in energy storage devices as the promising component of the electrode or solid electrolyte; the effect of molecular weight, crystallinity, and composite fabrication methods would be interesting aspects for further investigation.[19] On the contrary, the carboxylic acid (PAA) and amine (PEI) functional groups do not improve ionic interaction between the composite films and the electrolyte in this fabrication condition. **Figure 2b** displays the Bode phase plot from electrochemical impedance spectroscopy (EIS) measurements of PEDOTOH/gel electrodes in 1 M $LiClO_4$. All electrodes showed a similar phase angle of approximately -80° at low frequencies, signifying a capacitive behavior of the fabricated PEDOT/gel composites, in line with the CV results. In addition, the fitting of the Nyquist plots confirmed that the PEDOTOH/PEO has lower charge transfer resistance (R_{ct}) and higher double-layer capacitance (C_{dl}) as well as electrode capacitance (C_{mat}) than the native PEDOTOH, representing improved ionic conductivity at the interface of electrode-electrolyte and within the bulk of PEDOTOH/PEO electrode **(Figure S2, Table S1).**

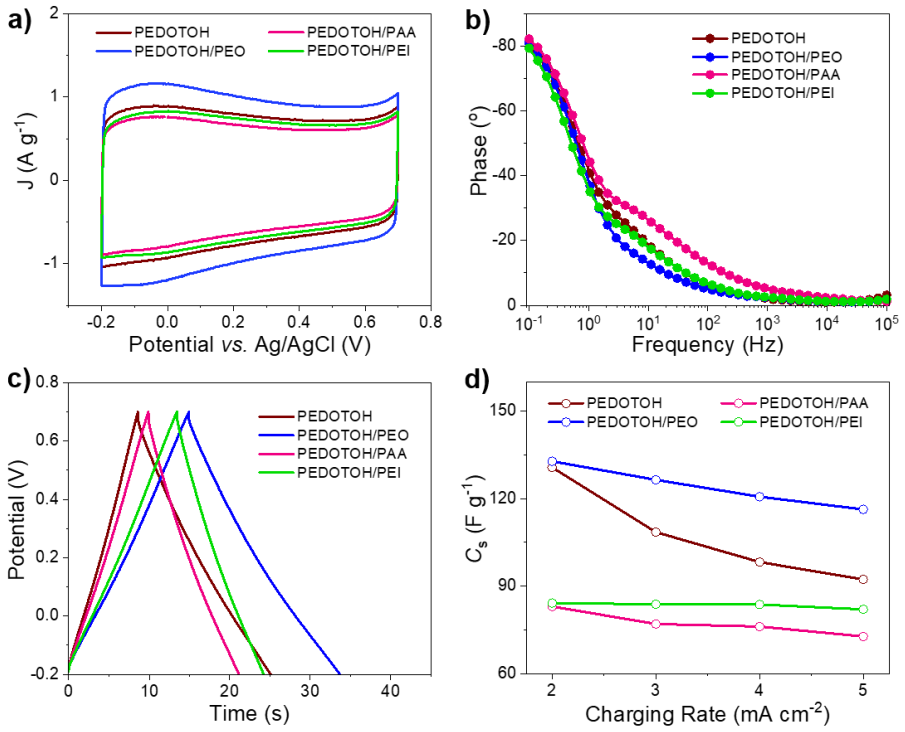

Figure 2. Electrochemical analysis of the PEDOTOH composite films. **(a)** CV curves at a scan rate of 10 mV s^{-1} over a potential window of -0.2 to 0.7 V *vs.* Ag/AgCl. **(b)** Phase of the impedance measured at 0 V *vs*. open circuit potential (V_{OC}). **(c)** Charge-discharge curves at 2 mA cm^{-2}. **(d)** Specific capacitance at different charging rates. All electrochemical measurements were performed in 1 M $LiClO_4$ at ambient conditions.

The specific capacitance of the PEDOTOH composite electrodes was determined by the discharge curve of galvanostatic charge-discharge cycles at different current densities (**Figure S3**). All electrodes exhibit ideal triangular shapes at any given current densities, consistent with the rectangular CV profiles that showed a dominated capacitive charge storage mechanism.[20] **Figure 2c** shows a comparative GCD plot at a current density of 2 mA cm^{-2}, and the specific capacitance extracted from GCD curves at different charging rates is presented in **Figure 2d**. The corresponding specific capacitances of each electrode as a function of normalized current density are shown in **Figure S4**. The PEDOTOH/PEO electrode delivers a specific capacitance of 132.8 F g^{-1} at a normalized current density of 6.4 A g^{-1} and reaches 116 F g^{-1} at a three-fold

higher current rate (e.g., 16 A g^{-1}), showing good rate capability. Conversely, the pristine PEDOTOH electrode demonstrates the lowest rate capability of all the electrodes investigated.

To elucidate the origin of the improved electrochemical properties of the gel composites, we evaluated the surface topography of the PEDOTOH films using scanning electron microscopy (SEM). The top view SEM images are displayed in **Figure 3a-d** and **Figure S5**. All PEDOTOH-based films, except the PEDOTOH/PAA, exhibit a rough surface with micrometer size agglomerates on their surface. In contrast, the PEDOTOH/PAA has a smooth surface. The PEDOTOH/PEI composite film presents a similar surface to the pristine PEDOTOH, whereas the PEDOTOH/PEO composite film displays a rougher surface and a greater number of agglomerates and grain-shape like structures. The SEM results imply that the type of incorporated gel could significantly affect the morphology of the polymer composites, leading to different electrochemical performances. This rougher surface of PEDOTOH/PEO film brings additional merits, such as a larger electrochemically active surface area, leading to superior specific capacitance. In addition, we calculate the electroactive surface area of PEDOTOH compared to PEDOTOH/PEO electrodes using the peak current method and the Randles-Sevcik equation to the CV curves measured in 3 mM $[Fe(CN)_6]^{4-}$ (**Figure S6**).[21] The electroactive surface area is 8.11 cm^2 and 5.67 cm^2 for PEDOTOH/PEO and PEDOTOH electrodes, respectively. Based on the improved capacitance and its distinct surface characteristics, the PEDOTOH/PEO composite represents the best performing composite sample in these fabrication conditions.

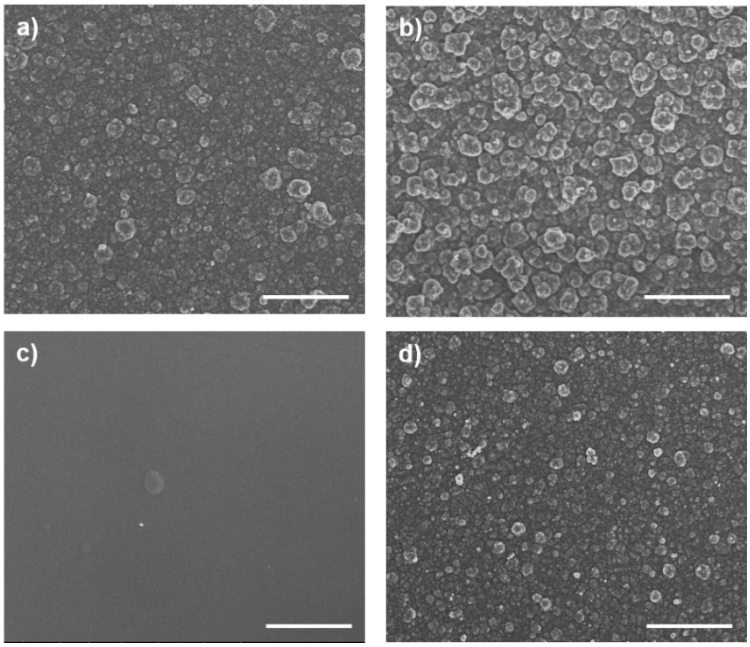

Figure 3. Top-view SEM images of (a) pristine PEDOTOH, (b) PEDOTOH/PEO, (c) PEDOTOH/PAA, and (d) PEDOTOH/PEI fabricated in aqueous solution. Scale bar is 10 μm.

The PEDOTOH/PEO electrodes were then assembled into symmetrical SCs immersed in agarose gel electrolytes. To identify the optimal gel composition, different supporting electrolytes such as 1 M $LiClO_4$, 1 M KOH, and 1 M H_2SO_4 were added to the agarose (6 wt%) in deionized water (10 mL). All SCs were examined under the same potential window at room temperature. **Figure 4a** shows the CV curves with different gel electrolytes at 10 mV s^{-1}. The CV curves of the SCs in agarose-$LiClO_4$ and agarose-H_2SO_4 are nearly rectangular, indicating a dominant capacitive behavior.[22] The specific capacitances calculated from the CV curves are 43.41 F g^{-1} and 43.98 F g^{-1} for agarose-$LiClO_4$ and agarose-H_2SO_4, respectively. This value is higher than several PEDOT-based SCs, such as PEDOT:PSS coated onto cellulose cloth (8.94 F g^{-1})[23] and printed stretchable GO-CNT-PEDOT (21.7 F g^{-1})[24] SCs. Interestingly, at a high scan rate (200 mV s^{-1}), the specific capacitance remains intact, achieving 43.37 F g^{-1} (agarose-$LiClO_4$) and 44.25 F g^{-1} (agarose-H_2SO_4). Therefore, these gel electrolytes support ion diffusion pathways while the electrodes maintain the active sites regardless of the increase in the scan rate. In addition, the CV curves retained a nearly rectangular shape even at a high scan rate of

200 mV s^{-1} (**Figure S7a-b**), indicating excellent capacitive behavior, which is further supported by the b-value from fitting the log(*J*) versus log(*v*) plots (**Figure S7d-e**). In contrast, in the case of the agarose-KOH electrolyte, we observed typical redox peaks in the CV curve around ± 0.25V at a scan rate of 10 mV s^{-1}, corresponding to a specific capacitance of 20.57 F g^{-1} (**Figure 4a**). The redox peak-to-peak separation on the CV curves becomes larger with increasing scan rate, indicating that the redox reaction becomes less efficient at high scan rates (**Figure S7c**) but is still governed by a capacitive-controlled process (**Figure S7f**). According to the literature, KOH could promote the over-oxidation reaction of PEDOT by inducing the formation of sulfone groups (-SO_2) and carbonyl groups (C=O) in the PEDOT chains with the presence of OH ions in the base environment.[25] Hence, the PEDOTOH/PEO composite electrode becomes less conducting in KOH electrolyte, hindering the performance of the SCs.

Further electrochemical evaluation using EIS and GCD cycling (**Figure 4b-c**, **Figure S8**) demonstrated that PEDOTOH/PEO-based SCs achieve the highest impedance and low charge capacity in the agarose-KOH gel electrolyte, attributed to the overoxidized PEDOTOH chain. The impedance values at low frequency (0.1 Hz) and the phase-angle profiles are quite similar for the SCs operated in agarose-$LiClO_4$ and agarose-H_2SO_4. However, the specific capacitance for the agarose-H_2SO_4 is slightly larger, particularly at higher rates compared to the agarose-$LiClO_4$, indicating a more facile ion transport of H_2SO_4, in line with the impedance values at a high frequency related to the electrolyte resistance (**Figure 4b**). It should be noted that the agarose-H_2SO_4 gel was not entirely solid-state due to the sulfation of the agarose by H_2SO_4.[26] We observed that the agarose-H_2SO_4 blend is more like a pre-gel state; thus, the H_2SO_4 ions come with greater freedom and mobility than $LiClO_4$ ions in the solid-state gel. Therefore, we concluded that suitable supporting electrolytes for forming the agarose gel electrolyte for PEDOT-based SCs should occur at neutral pH. Basic compounds might induce over-oxidation of the PEDOT chain, while the acidic substances, as in this case of H_2SO_4, can react with the

agarose gel (e.g., sulfation). Hence, based on the result from electrochemical measurements and the physical stability of the forming a solid-state agarose gel electrolytes, we selected the agarose-$LiClO_4$ as the optimal blend combination.

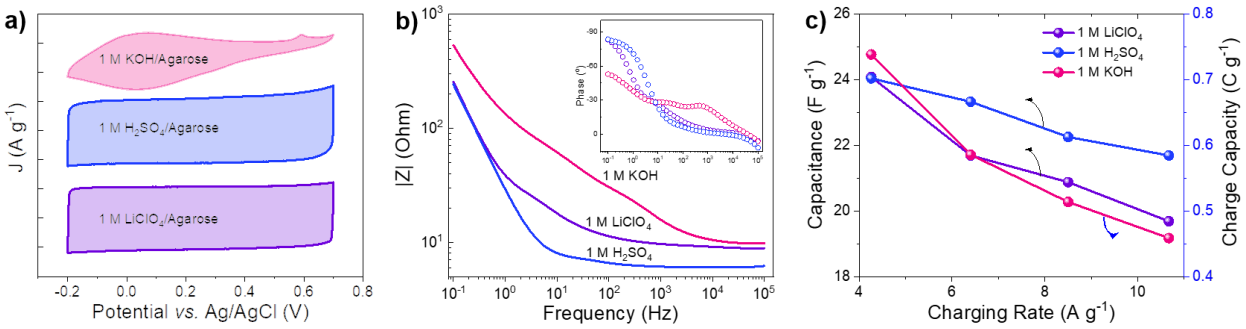

Figure 4. Electrochemical performance of the PEDOTOH/PEO-based supercapacitors with different electrolytes. **(a)** CV curves at a scan rate of 10 mV s^{-1}. **(b)** Bode plot of the supercapacitors at 0 V *vs.* operating-circuit potential (V_{OC}). **(c)** Specific capacitances at different charging rates.

We then further explored the performance of PEDOTOH/PEO-based SCs by varying the concentration of $LiClO_4$ in the agarose gel. The salt concentration hinges on SCs voltage window, electrochemical stability, viscosity, and ionic conductivity of the electrolyte.[27] Low electrolyte salt concentrations typically exhibit slow cycling speed and counter-ion adsorption; on the other hand, if the salt concentration is too high, the cations and anions prefer to associate strongly and thus reduce the number of free ions leading to a decrease in the electrolyte conductivity.[27-28] Here, we examined three concentrations of $LiClO_4$, namely 0.5, 1, and 2 M. The CV curves remain nearly rectangular with identical current density, independent of the $LiClO_4$ loading in the gel electrolytes (**Figure S9a**). The Bode plots reveal a difference at high frequencies. Generally, the high frequency corresponds to the solution resistance of the system. The solution resistance increases in the lowest concentration of 0.5 M and becomes similar as

the concentration increases from 1 to 2 M (**Figure S9b**). The phase angle curves in the inset of **Figure S9b** show the same trend for all concentrations.

Then, the charge-discharge tests of the SCs with 0.5 to 5 M $LiClO_4$ in agarose gel were compared, as illustrated in **Figure S10**; all the GCD plots display ideal triangle curves. The corresponding specific capacitance values extracted from the GCD plots are presented in **Figure 5a**. The SCs operated in a higher concentration of $LiClO_4$ exhibit an increase in the specific capacitances over the range of charging rates tested (**Figure S11**). The device with 1 M electrolyte (25.5 F g^{-1}) shows a slight increase in specific capacitance at a low charging rate (2.1 A g^{-1}) compared to 0.5 M electrolyte (24.9 F g^{-1}), suggesting that higher $LiClO_4$ concentration in the agarose gel electrolyte could enhance the capacitance properties of the PEDOTOH/PEO SCs, in agreement with previous studies reporting better capacitances using higher electrolyte concentration for activated carbon[29] and graphene SCs[30].

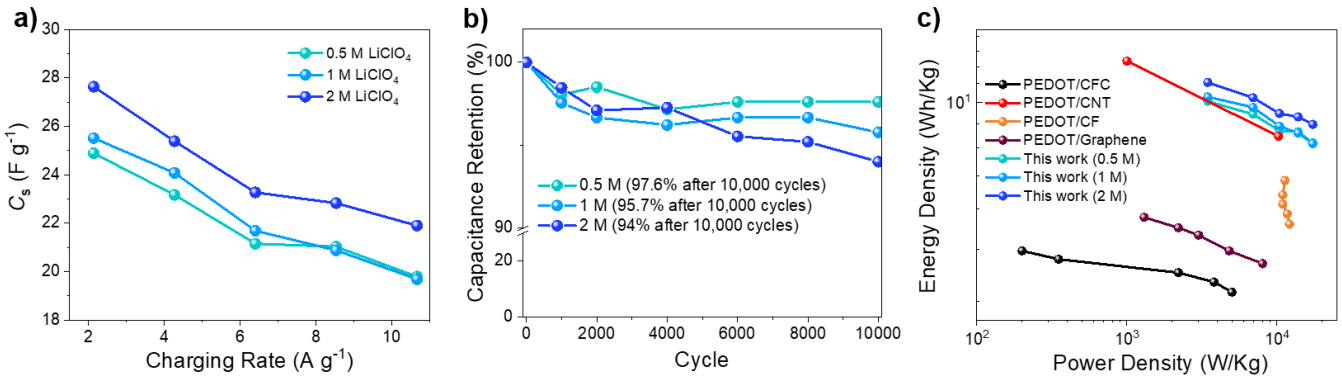

Figure 5. Electrochemical performance of the PEDOTOH/PEO-based supercapacitors with different concentrations of $LiClO_4$-agarose electrolytes. **(a)** Specific capacitances at different charging rates, calculated from GCD plots. **(b)** Cycling stability tested at 10.67 A g^{-1} over 10000 cycles. **(c)** Comparative Ragone plots of the PEDOTOH/PEO supercapacitors compared to other PEDOT-based supercapacitors.

Finally, we investigated the cycling stability of the PEDOTOH/PEO-based SCs in these electrolyte concentrations, displayed in **Figure 5b**. The SCs showed remarkable stability over 10,000 cycles, with negligible capacitance fade (2-6%) and high coloumbic efficiency (~100%) (**Figure S12**). The maximum energy density of an SC comprising 2 M $LiClO_4$-agarose reached 11.19 Wh $Kg^{-1,}$ and the maximum power density was ca. 17.28 kW Kg^{-1}. This PEDOTOH/PEO-based SCs in agarose-$LiClO_4$ electrolyte is superior to PEDOT/CNT, PEDOT/graphene, and PEDOT/Carbon Fiber SC devices as shown in the Ragone plot in **Figure 5c**.[31] The performance of PEDOTOH/PEO-based SCs in agarose-$LiClO_4$ is among the highest compared to other PEDOT-based SCs, with remarkable retention under a high charging rate (**Table S2**).

Conclusions

In summary, we demonstrated a comparative study to evaluate the effect of incorporated hydrogels and the optimal agarose gel electrolyte on the performance of PEDOTOH-based supercapacitors. Three appealing hydrogels, namely PEO, PAA, and PEI, were incorporated into PEDOTOH networks *via* a single-step electrochemical polymerization in an aqueous solution. The PEDOTOH/PEO composite exhibit the highest specific capacitance of 195.2 F g^{-1} at a scan rate of 10 mV s^{-1}, which is 93% of the theoretical capacity of PEDOT (210 F g^{-1}). The PEDOTOH/PEO electrodes were then assembled into a symmetrical supercapacitor in an agarose gel with different supporting electrolytes and varying concentrations. The supercapacitors comprising 2 M $LiClO_4$-agarose achieved a specific capacitance of 27.6 F g^{-1} at a current density of 2 A g-1, a superior cyclability of ~94% after 10,000 charge/discharge cycles at 10.6 A g^{-1}, the maximum energy density of 11.2 Wh kg^{-1} and maximum power density of 3.45 kW kg^{-1}. This work highlights a simple fabrication protocol for PEDOTOH/gel composite as an alternative electrode for high-performance PEDOT-based supercapacitors.

Experimental Section

Materials

Hydroxymethyl 3,4-ethylenedioxythiophene (EDOTOH, 95%, CAS: 146796-02-3), lithium perchlorate ($LiClO_4$, 99.99%, CAS: 7791-03-9), poly(ethylene oxide) (PEO, M_v ~1,000,000, CAS: 25322-68-3), poly(acrylic acid) (PAA, M_v ~450,000, CAS: 9003-01-4), polyethyleneimine (PEI, CAS: 9002-98-6), agarose, potassium hydroxide (KOH, ≥85%, CAS: 1310-58-3), and sulfuric acid (H_2SO_4, 95.0-98.0%, CAS: 7664-93-9) was purchased from Sigma-Aldrich, and used as received. The aqueous solutions were prepared using ultrapure water (Millipore Milli-Q).

Electropolymerization of the PEDOTOH electrodes

We prepared an aqueous dispersion of 10 mM of EDOTOH monomers and 100 mM of $LiClO_4$ as counteranions. These dispersions are sonicated at room temperature for 30 min, and then used as the reaction electrolyte during three-electrode electrochemical polymerization onto Au sputtered Kapton substrates (polyimide). A platinum wire and an Ag/AgCl were immersed into the solution and used as the counter and reference electrodes, respectively. We performed a potentiostatic electropolymerization mode at 1 V for 300 s on 8 mm x 8 mm Au/Kapton substrates (geometrical surface area = 0.64 cm^2). Then, we washed the electropolymerized PEDOTOH electrodes with deionized water and dried them with N_2 spray to remove any weakly bound material and unreacted monomers. For the fabrication of PEDOT/gel electrodes, we mixed 5 wt% of PEO, PAA or PEI into the monomer dispersion prior to electrodeposition.

Preparation of gel electrolyte and assembly of the supercapacitors

The agarose gel electrolytes were prepared according to the procedure in the previous study.[32] First, 600 mg agarose (6 wt%) were dissolved in 10 mL DI water by continuous stirring at 90

^{0}C until homogeneous mixture was obtained. 1.06 g $LiClO_4$, 561 mg KOH, and 546 µL 98% H_2SO_4 were added to obtain 1 M $LiClO_4$-agarose, 1 M KOH-agarose, and 1 M H_2SO_4-agarose, respectively. Then, the two PEDOTOH/PEO electrodes were assembled in the gel electrolyte with a distance of 2 mm. The gel electrolyte serves as an ion diffusion pathway, separator and binding medium of the cathode and anode electrodes.

Electrochemical characterization

Electrochemical measurements of deposited polymer electrodes as working electrodes were performed using the three-electrode configuration in 1 M $LiClO_4$ at room temperature. Ag/AgCl and Pt wire were used as reference electrodes and counter electrodes, respectively. The electrochemical properties such as specific capacitance and cycling stability were evaluated by cyclic voltammetry (CV) and galvanostatic charge-discharge (CGD). The specific capacitance of the electrodes and the assembled supercapacitors were calculated from either CV at a specific scan rate or GCD at a set current density. The specific capacitance (C_s, F g^{-1}), which is the capacitance of one electrode per unit mass, was calculated using the following equations from CV curves (**Eq. 1**) and GCD plots (**Eq. 2**),

$$Cs = \frac{Q}{2\mu\Delta V} \quad \textbf{(1)}$$

$$Cs = \frac{i\,\Delta t}{\Delta V} \quad \textbf{(2)}$$

where Q is the total charge in coulombs by calculating the integral area of the CV curve, μ and ΔV represent the scan rate and the potential window of the CV cycle, respectively. For equation 2, i is the discharge current density (A g^{-1}), Δt and ΔV are the discharge time and potential window, respectively. In addition, the capacitance retention of the electrode and supercapacitors was evaluated by using CV and GCD for multiple cycles within a potential window lying between -0.2 to 0.7 V. The energy density (E, Wh kg^{-1}) and the power density (P, W kg^{-1}) were extracted from the GCD curves from the following equations:

$$E = \frac{C_S\,(\Delta V)^2}{2} \quad \textbf{(3)}$$

$$P = \frac{E\,x\,3600}{\Delta t} \quad \textbf{(4)}$$

The coulombic efficiency ($n_{coulombic}$) of the supercapacitors was evaluated as the ratio between the discharging and charging times within -0.2 and 0.7 V as displayed below:

$$n_{coulombic} = \frac{Total\ charge\ released}{Total\ charge\ stored} = \frac{Discharging\ time}{Charging\ time} \quad \textbf{(5)}$$

Electrochemical impedance spectroscopy (EIS) for the electrodes and supercapacitor devices was examined at the open-circuit potential. The AC amplitude was 10 mV, while the frequencies varied between 0.1 Hz and 100 kHz.

Physicochemical characterization

We examined the surface morphology of the PEDOTOH composite films using FEI Nova nano scanning electron microscope (SEM) with an accelerating voltage of 3 kV and a working distance of 5 mm. The coated polymer films on gold/kapton substrates were mounted onto aluminum stubs and attached with conductive double-sided tape. We performed X-ray photoelectron spectroscopy (XPS) and Fourier transform infrared (FTIR) studies To characterize the chemical composition of the polymer films. XPS was performed using a KRATOS Analytical AMICUS instrument equipped with an achromatic Al Kα X-ray source (1468.6 eV). The source was operated at a voltage of 10 kV and a current of 10 mA generating a power of 100 Watts. The high-resolution XPS spectra were acquired using a step of 0.1 eV. The pressure in the analysis chamber was in the range of × 10^{-7} Pa during the course of the measurements. Whereas, we recorded the FTIR spectra in the range 550-4000 cm^{-1} at room temperature using Thermo Scientific Nicolet iS10. We used attenuated total reflection (ATR) FTIR mode to obtain the reflectance infrared spectra of the polymer film. We signal-averaged

64 scans to form a single spectrum which was then displayed in terms of transmittance, and the baseline was corrected using OMNIC FTIR software.

Supporting Information

Supporting Information is available from the Wiley Online Library or from the author.

Acknowledgments

S.W. acknowledges a research grant program supported by Institut Teknologi Bandung (ITB) under contract number 0681/IT1.B05/KP/2021.

Received: ((will be filled in by the editorial staff))
Revised: ((will be filled in by the editorial staff))
Published online: ((will be filled in by the editorial staff))

References

[1] M. Yaseen, M. A. K. Khattak, M. Humayun, M. Usman, S. S. Shah, S. Bibi, B. S. U. Hasnain, S. M. Ahmad, A. Khan, N. Shah, A. A. Tahir and H. Ullah, *Energies* **2021**, *14*, 7779.
[2] S. M. Rezaei Niya and J. Andrews, *Electrochimica Acta* **2022**, *402*, 139534.
[3] a) Y. Wang, Y. Ding, X. Guo and G. Yu, *Nano Research* **2019**, *12*, 1978-1987; b) Y. Han and L. Dai, *Macromolecular Chemistry and Physics* **2019**, *220*, 1800355.
[4] K. Sun, S. Zhang, P. Li, Y. Xia, X. Zhang, D. Du, F. H. Isikgor and J. Ouyang, *Journal of Materials Science: Materials in Electronics* **2015**, *26*, 4438-4462.
[5] Z. Zhao, G. F. Richardson, Q. Meng, S. Zhu, H.-C. Kuan and J. Ma, *Nanotechnology* **2015**, *27*, 042001.
[6] S. Khasim, A. Pasha, N. Badi, M. Lakshmi and Y. K. Mishra, *RSC Advances* **2020**, *10*, 10526-10539.
[7] Q. Xu, C. Lu, S. Sun and K. Zhang, *Journal of Physics and Chemistry of Solids* **2019**, *129*, 234-241.
[8] a) C. Li, S. Wang, Y. Cui, X. Wang, Z. Yong, D. Liang, Y. Chi and Z. Wang, *ACS Applied Materials & Interfaces* **2022**, *14*, 9172-9182; b) L. Li, N. Zhang, M. Zhang, X. Zhang

and Z. Zhang, *Dalton Transactions* **2019**, *48*, 1747-1756; c) L. Qin, Q. Tao, A. El Ghazaly, J. Fernandez-Rodriguez, P. O. Å. Persson, J. Rosen and F. Zhang, *Advanced Functional Materials* **2018**, *28*, 1703808.
[9] Y. Gao, *Nanoscale Research Letters* **2017**, *12*, 387.
[10] Q. Liu, J. Qiu, C. Yang, L. Zang, G. Zhang and E. Sakai, *Advanced Materials Technologies* **2021**, *6*, 2000919.
[11] -. F. SUN, -. Y. PAN, -. Y. ZHANG, -. H. LIU and -. F. DU, - *Acta Materiae Compositae Sinica* **2022**, - *39*, - 1131.
[12] S. Alipoori, S. Mazinani, S. H. Aboutalebi and F. Sharif, *Journal of Energy Storage* **2020**, *27*, 101072.
[13] H. Dai, G. Zhang, D. Rawach, C. Fu, C. Wang, X. Liu, M. Dubois, C. Lai and S. Sun, *Energy Storage Materials* **2021**, *34*, 320-355.
[14] S. T. Senthilkumar, R. K. Selvan, J. S. Melo and C. Sanjeeviraja, *ACS Applied Materials & Interfaces* **2013**, *5*, 10541-10550.
[15] C. Ramasamy, J. Palma del vel and M. Anderson, *Journal of Solid State Electrochemistry* **2014**, *18*, 2217-2223.
[16] a) Z. S. Parr, R. B. Rashid, B. D. Paulsen, B. Poggi, E. Tan, M. Freeley, M. Palma, I. Abrahams, J. Rivnay and C. B. Nielsen, *Advanced Electronic Materials* **2020**, *6*, 2000215; b) P. Li and T. Lei, *Journal of Polymer Science* **2022**, *60*, 377-392; c) C.-Y. Yang, M.-A. Stoeckel, T.-P. Ruoko, H.-Y. Wu, X. Liu, N. B. Kolhe, Z. Wu, Y. Puttisong, C. Musumeci, M. Massetti, H. Sun, K. Xu, D. Tu, W. M. Chen, H. Y. Woo, M. Fahlman, S. A. Jenekhe, M. Berggren and S. Fabiano, *Nature Communications* **2021**, *12*, 2354; d) F. Fu, J. Wang and J. Yu, *Journal of Materials Chemistry C* **2021**, *9*, 11794-11800; e) A. Parodi, S. M. Khaled, I. K. Yazdi, M. Evangelopoulos, N. E. T. Furman, X. Wang, F. Urzi, S. Hmaidan, K. A. Hartman and E. Tasciotti in *Smart Hydrogels*, (Ed. B. Bhushan), Springer Netherlands, Dordrecht, **2016**, pp. 3735-3747.
[17] a) S. Wustoni, T. C. Hidalgo, A. Hama, D. Ohayon, A. Savva, N. Wei, N. Wehbe and S. Inal, *Advanced Materials Technologies* **2020**, *5*, 1900943; b) C.-L. Lin, C.-Y. Chen, H.-F. Yu and K.-C. Ho, *Solar Energy Materials and Solar Cells* **2019**, *202*, 110132; c) S. Zhang, J. Xu, B. Lu, L. Qin, L. Zhang, S. Zhen and D. Mo, *Journal of Polymer Science Part A: Polymer Chemistry* **2014**, *52*, 1989-1999; d) Y. Xiao, X. Cui, J. M. Hancock, M. Bouguettaya, J. R. Reynolds and D. C. Martin, *Sensors and Actuators B: Chemical* **2004**, *99*, 437-443; e) Y. Lu, Y.-p. Wen, B.-y. Lu, X.-m. Duan, J.-k. Xu, L. Zhang and Y. Huang, *Chinese Journal of Polymer Science* **2012**, *30*, 824-836.
[18] A. Giovannitti, D.-T. Sbircea, S. Inal, C. B. Nielsen, E. Bandiello, D. A. Hanifi, M. Sessolo, G. G. Malliaras, I. McCulloch and J. Rivnay, *Proceedings of the National Academy of Sciences* **2016**, *113*, 12017-12022.
[19] a) A. Apicella, B. Cappello, M. A. Del Nobile, M. I. La Rotonda, G. Mensitieri and L. Nicolais, *Biomaterials* **1993**, *14*, 83-90; b) J. Cheng, G. Hou, Q. Chen, D. Li, K. Li, Q. Yuan, J. Wang and L. Ci, *Chemical Engineering Journal* **2022**, *429*, 132343; c) J. Yang, L. Shao, X. Wang, Y. Yang, Z. Tian, W. Chen, G. Zhang and C. Shen, *Journal of Alloys and Compounds* **2020**, *845*, 155179.
[20] G. Nikiforidis, S. Wustoni, C. Routier, A. Hama, A. Koklu, A. Saleh, N. Steiner, V. Druet, H. Fiumelli and S. Inal, *Macromolecular Bioscience* **2020**, *20*, 2000215.
[21] P. Zhu and Y. Zhao, *Materials Chemistry and Physics* **2019**, *233*, 60-67.
[22] S. Amara, W. Zaidi, L. Timperman, G. Nikiforidis and M. Anouti, *The Journal of Chemical Physics* **2021**, *154*, 164708.
[23] L. Manjakkal, A. Pullanchiyodan, N. Yogeswaran, E. S. Hosseini and R. Dahiya, *Advanced Materials* **2020**, *32*, 1907254.
[24] Y. Zhou, C. B. Parker, P. Joshi, A. K. Naskar, J. T. Glass and C. Cao, *Advanced Materials Technologies* **2021**, *6*, 2001055.

[25] P. Tehrani, A. Kanciurzewska, X. Crispin, N. D. Robinson, M. Fahlman and M. Berggren, *Solid State Ionics* **2007**, *177*, 3521-3527.
[26] a) R. Takano, S. Yoshikawa, T. Ueda, K. Hayashi, S. Hirase and S. Hara, *Journal of Carbohydrate Chemistry* **1996**, *15*, 449-457; b) H. Yasunaga, R. Koga, R. Takano, K. Kajiwara and H. Urakawa, *Sen'i Gakkaishi* **2006**, *62*, 293-296; c) T. Fuse and T. Suzuki, *Agricultural and Biological Chemistry* **1975**, *39*, 119-126.
[27] B. Pal, S. Yang, S. Ramesh, V. Thangadurai and R. Jose, *Nanoscale Advances* **2019**, *1*, 3807-3835.
[28] a) C. Prehal, C. Koczwara, H. Amenitsch, V. Presser and O. Paris, *Nature Communications* **2018**, *9*, 4145; b) C.-H. Wang, Y.-W. Yeh, N. Wongittharom, Y.-C. Wang, C.-J. Tseng, S.-W. Lee, W.-S. Chang and J.-K. Chang, *Journal of Power Sources* **2015**, *274*, 1016-1023.
[29] a) Y. Tian, J.-W. Yan, R. Xue and B.-L. Yi, *Acta Physico-Chimica Sinica* **2011**, *27*, 479-485; b) G. Nikiforidis, M. E. Yagoubi and M. Anouti, *Electrochimica Acta* **2022**, *402*, 139529.
[30] Q. Chen, X. Li, X. Zang, Y. Cao, Y. He, P. Li, K. Wang, J. Wei, D. Wu and H. Zhu, *RSC Advances* **2014**, *4*, 36253-36256.
[31] a) M. Rajesh, C. J. Raj, R. Manikandan, B. C. Kim, S. Y. Park and K. H. Yu, *Materials Today Energy* **2017**, *6*, 96-104; b) X. He, W. Yang, X. Mao, L. Xu, Y. Zhou, Y. Chen, Y. Zhao, Y. Yang and J. Xu, *Journal of Power Sources* **2018**, *376*, 138-146; c) G. P. Pandey, A. C. Rastogi and C. R. Westgate, *Journal of Power Sources* **2014**, *245*, 857-865; d) S. Ahmed, M. Rafat, M. K. Singh and S. A. Hashmi, *Nanotechnology* **2018**, *29*, 395401.
[32] G. Nikiforidis, S. Wustoni, D. Ohayon, V. Druet and S. Inal, *ACS Applied Energy Materials* **2020**, *3*, 7896-7907.

A functional PEDOT/gel for supercapacitors: This work examines the electrochemical performance of PEDOTOH/gel composites fabricated via a single-step electropolymerization technique in an aqueous solution. The best performing PEDOTOH/PEO composite is applied as electrode material for symmetrical supercapacitors in agarose gel electrolyte, demonstrating excellent long-term cycling stability with a capacitance loss of only 6% after 10000 cycles at a high current density of 10.6 A g^{-1}.

PEDOT, Electropolymerization, Agarose, Gel Electrolyte, Supercapacitors.

S. Wustoni,* G. Nikiforidis, D. Ohayon, S. Inal, Y.S. Indartono, V. Suendo, B. Yuliarto

Performance of PEDOTOH/PEO-based Supercapacitors in Agarose Gel Electrolyte